M. D. Frederick, R. M. Gejji, J. E. Shepherd, and C. D. Slabaugh. Reactive processes following transverse wave interaction. Proceedings of the Combustion Institute, 2024. Preprint of Supplemental Material for article accepted for publication in the proceedings of the 40th International Symposium on Combustion, Milan, ITALY, July 21-26, 2024.

Supplementary Material: Reactive processes following transverse wave interaction

Mark D. Frederick, J.E. Shepherd, Rohan M. Gejji, Carson D. Slabaugh

The purpose of this supplement is to provide context and the mathematical details of the modeling of reaction behind an unsteady, curved shock front, discuss the approximations involved, and analyze two examples of unsteady detonation fronts discussed in the main article. A concise summary of the results in provided by presenting the results in terms of the expansion time scale compared to critical values computed from detailed reaction models.

1 Introduction

There are three main ingredients to approximate analysis of reaction zones behind unsteady shock waves.

1. A model for the unsteady reaction zone following a curved shock.
2. A set of compatibility or shock change relations coupling the gradients, curvature, and time rate of change of properties with shock unsteadiness as characterized by the acceleration $\mathrm{d}U/\mathrm{d}t$.
3. A set of empirical relationships for shock speed, acceleration, and wave curvature derived either from numerical simulations or experimental data for $U(t)$ and $R(t)$.

The key idea in the simplest models of the unsteady reaction zone is to use a control volume model of the energy equation with a prescribed volume expansion rate. The volume expansion rate can be estimated in one of two ways.

1. Assuming a shock trajectory $R(t)$ and specified time dependence of properties along a path line.
2. Assuming that the contributions of unsteadiness and lateral flow divergence due to curvature are constant along path lines and given by the values at the shock front as determined by the shock change relationships.

The key result of the model is that rate of change of temperature along a path line behind a decaying, curved shock is a competition between energy release by chemical reaction $\mathrm{d}Y_k/\mathrm{d}t$, and volume expansion

$$\boxed{\frac{\mathrm{D}T}{\mathrm{D}t} = -\frac{1}{c_v}\sum_k e_k \frac{\mathrm{D}Y_k}{\mathrm{D}t} - \frac{RT}{c_v}\frac{1}{v}\frac{\mathrm{D}v}{\mathrm{D}t}}$$

In general the volume expansion $v(t)$ is a function of time along a path line. The gist of the model we use is to approximate the expansion rate as a constant determined by the value at time the path line passes through the the shock front. We use the shock change equations to define an expansion time scale τ_v.

$$\boxed{\frac{1}{\tau_v} \equiv \frac{1}{v}\frac{\mathrm{D}v}{\mathrm{D}t} = -A\frac{\mathrm{d}M_s}{\mathrm{d}t} - Ba_1\kappa}$$

The coefficients A and B are $O(1)$ nondimensional functions of the shock speed or equivalently shock Mach number $M_s = \mathrm{U}/a_1$ and mixture thermodynamics. The temperature equation is coupled to the evolution of the species as determined by a reaction network model and a closure assumption is required to relate thermodynamic properties on the path line.

A critical level of competition between energy release and flow work is characterized by a *critical expansion time* τ_v. When the time is smaller than a critical value,

$$\boxed{\tau_v < \tau_v^* \quad \text{quenching}}$$

the induction time becomes infinite and the reaction is decoupled from the leading shock. This is observed in both detailed and simplified reaction models. Using a detailed reaction model, realistic thermochemistry, and experimental results for shock speed and curvature, we evaluate the coefficients A and B, and compute the evolution of temperature along selected path lines for two cases. The critical decay times are evaluated and found to be dominated by the contribution from shock unsteadiness for the cases we examine. The results of the path line analysis are compared to the critical decay time criteria and are shown to be in good agreement.

1.1 Background

The approach we take to modeling reaction behind unsteady, curved shock waves, is based on Eckett et al. (2000). Many other researchers have considered this topic, and we provide in this section an appreciation of these contributions and some historical context.

The role of unsteadiness in detonation fronts was recognized following the first observations of unstable structure of the front (Fickett and Davis, 1979, Lee, 2008) in the 1950s. Acknowledging the discussion by Soloukhin (1969) on the effect of unsteadiness on the coupling between the shock front and chemical reaction, Lundstrom and Oppenheim (1969) used a blast wave model of the transient leading shock fronts in a cellular detonation to demonstrate how the sensitivity of chemical reactions to temperature could lead to decoupling of the shock and reaction fronts. Eckett et al. (2000) examined the effect of nonsteadiness on the initiation of the detonation by blast waves with computational fluid dynamics modeling of unsteady one-dimensional flows. Analyses of the results on pathlines led to the development of the critical decay rate model and predictions of critical energy for detonation initiation. Subsequently, Austin et al. (2005a,b) applied this model to simulations of cellular structure by (Gamezo et al., 1999a,b). Jackson et al. (2019), Jackson and Short (2013) analyzed experimental and numerical simulations of cellular detonation and observed that in some cases a unique relationship between shock speed, acceleration and curvature could be found. Most recently, Cheevers (2021) has carried out analyses with a approach similar to the present study to examine the effect of shock acceleration and curvature using experimental data for two mixtures: $2H_2 + O_2 + 7Ar$ and $CH_4 + 2O_2$.

A number of researchers have independently used similar methodologies to consider the effect of unsteadiness on ignition. Vázquez-espí and Liñán (2001) considered the problem of homogeneous, non-diffusive ignition with rapid, concentrated deposition of energy. They identified a critical condition associated with the competition between expansion waves and chemical energy release that determined if thermal runaway would occur. Vidal and Khasainov (1999) considered the ignition behind unsteady shock waves and identified a critical condition for ignition this is essentially identical to that used in the present study: the rate of heat release has to exceed the rate of volume expansion. The role of unsteadiness in transient jet initiation of combustion was considered in depth by Radulescu and Law (2007), Radulescu and Maxwell (2010), Maxwell and Radulescu (2011) who formulated ignition criteria in terms of a competition between volume expansion and energy release by chemical reaction. The transient ignition due to water hammer compression events Coronel et al. (2020) in pipelines was analyzed using these concepts by Shepherd (2020). Recently, Tan et al. (2023) have reviewed a number of studies applying the concepts of unsteady ignition modeling.

The approach we used of focusing on the processes just behind the wave

front to obtain an evolution equation for the wave strength is known as the *shock change equation*. Versions of the shock change or acceleration wave formalism has been derived independently by a number of researchers over the past century as discussed by Becker (1972) and Chen and Gurtin (1971). The results have been used to analyze the growth and decay of shock waves in inhomogeneous (Nunziato and Walsh, 1972, 1973) and chemically reacting flows (Nunziato, 1973, Kennedy and Nunziato, 1976). Fickett and Davis (1979, p. 101) discuss the application to detonations and the implications for steady flow in the reaction zone. Recently, Radulescu (2020) derived expressions for shock propagation in quasi-one dimensional flows, gave explicit expressions for nonreactive perfect gases and discussed the relationship to the shock dynamics approximation of Whitham. Extension to fully three-dimensional shock fronts was given by Rabie and Wackerle (1978) defining the local shock shape with principle radii of curvature. Emanuel (2013) discusses in great detail the computation of spatial derivatives for curved shocks in a perfect gas; there is brief mention of unsteadiness but no consideration of reaction processes.

2 Unsteady Reaction Zone Models

The analyses of Eckett et al. (2000) and Arienti and Shepherd (2005) of reaction zones behind decaying blast waves in one and two dimensions examined the dominate balance along path lines in the reaction zone and divided contributions into terms representing the effects of chemical reaction (effective heat release), stream tube divergence (curvature), and unsteadiness. The balance equations along a streamline behind a propagating shock appear identical in form to the shock change relations but the terms apply throughout flow, not just at the shock front. For example, (2.6c) of Eckett et al. (2000) describes the evolution of the pressure along a particle path with downstream distance from a spherical shock (radius R_s and velocity U) measured by $x = R_s(t) - r$ and with relative velocity $w = U(t) - \mathrm{u}(r,t)$, $U = \mathrm{d}R_s/\mathrm{d}t$. The equations of motion in the (x,t) coordinates are:

$$\eta \frac{\mathrm{D}P}{\mathrm{D}t} = -\rho w^2 \dot{\sigma} + \frac{j}{R_s - x}\rho w^2 (U - w) + \rho w \frac{\mathrm{d}U}{\mathrm{d}t} - \rho w \frac{\partial w}{\partial t} + \frac{\partial P}{\partial t} \,. \tag{1}$$

where the sonic parameter is defined using the frozen (fixed chemical composition) sound speed a_f

$$\eta = 1 - w^2/a_f^2 \tag{2}$$

The corresponding density equation is

$$\eta\frac{\mathrm{D}\rho}{\mathrm{D}t} = -\rho\dot{\sigma} + \frac{1}{a^2}\left[\frac{j}{R_s - x}\rho w^2(U-w) + \rho w\frac{\mathrm{d}U}{\mathrm{d}t} - \rho w\frac{\partial w}{\partial t} + \frac{\partial P}{\partial t}\right], \quad (3)$$

and the velocity equation is

$$\eta\frac{\mathrm{D}w}{\mathrm{D}t} = w\dot{\sigma} - \frac{j}{R_s - x}w(U-w) - \left(\frac{w}{a}\right)^2\frac{\mathrm{d}U}{\mathrm{d}t} + \frac{\partial w}{\partial t} - \frac{w}{\rho a^2}\frac{\partial P}{\partial t}, \quad (4)$$

The species evolution equation transforms without any addition terms

$$\frac{\mathrm{D}Y_k}{\mathrm{D}t} = \Omega_k\,. \quad (5)$$

In this coordinate system, the substantial derivative is

$$\frac{\mathrm{D}(\cdot)}{\mathrm{D}t} = \frac{\partial(\cdot)}{\partial t} + w\frac{\partial(\cdot)}{\partial x}\,. \quad (6)$$

The approximate control volume model of the reaction along the fluid path lines is formulated in terms of temperature. The exact evolution equation for temperature behind a spherical blast wave is

$$\eta\frac{\mathrm{D}T}{\mathrm{D}t} = T(1-\gamma M^2)\dot{\sigma} - \eta T\sum_k \frac{\mathcal{W}}{\mathcal{W}_k}\Omega_k + \frac{1}{\rho c_p}\left[\frac{j}{R_s - x}\rho w^2(U-w) + \rho w\frac{\mathrm{d}U}{\mathrm{d}t} - \rho w\frac{\partial w}{\partial t} + \frac{\partial P}{\partial t}\right]. \quad (7)$$

where $M = w/a$ is the downstream flow Mach number in the shock reference frame and $\gamma = c_p/c_v$ is the (frozen) ratio of specific heats. The thermicity (for an ideal gas) can be expressed as

$$\dot{\sigma} = \sum_k \left(\frac{\mathcal{W}}{\mathcal{W}_k} - \frac{h_k}{c_p T}\right)\Omega_k \quad (8)$$

or equivalently

$$\dot{\sigma} = \frac{1}{\gamma}\sum_k \left(\frac{\mathcal{W}}{\mathcal{W}_k} - \frac{e_k}{c_v T}\right)\Omega_k \quad (9)$$

At the shock front, $x = 0$, (1) identical with (36) and this is also the case for the ρ and w evolution equations. Downstream of the front, these equations are an exact transformation of the unsteady, one-dimensional reactive

flow equations. However, this system of equations is not closed for a given streamline even if we are given a prescription for the blast wave trajectory $R_s(t)$. The partial derivatives with respect to time of P and w depend on the time variation on adjacent streamlines at a fixed x location, information that can only be reliably found by direct simulation of the entire flow field using the reactive Euler equations. However, this formulation is useful for analyzing direct simulations and serves as motivation for approximate models based on estimating the time derivatives.

Analyzing several cases of direct numerical simulation of decaying, reactive blast waves with a simple chemical reaction models, Eckett et al. (2000) proposed an approximate model of the reaction zone based on examining the magnitude of the terms in (1 - 5) for path lines leaving the shock near the time when the reaction was quenched due to the decay of the blast wave. For sufficiently large shock wave radii, the dominant balance was found to be between unsteadiness and chemical energy release with lateral (stream tube) expansion playing a minor role. An approximate model was developed using a constant value of the unsteadiness contribution and neglecting the curvature contribution. An asymptotic analysis of this approximate model revealed that there existed a critical magnitude of the unsteadiness that determined when the reaction was quenched. This *critial decay rate* model was applied to the problem of direct initiation of detonations by point energy sources to estimate the magnitude of minimum energy required to establish a self-sustaining detonation. The idea of competition between unsteadiness and chemical energy release has subsequently been applied to other situations such ignition by transient compression events (Shepherd, 2020).

Approximate reaction zone structure equations can be formulated by recognizing that the right-hand side of (36) represents the quasi-steady, thin reaction zone model terms and the left-hand side as contribution of the unsteadiness of the shock wave. If approximations for the unsteady and curvature terms can be found, then these reaction zone equations can be integrated to determine the effect of contributions on the reaction zone structure along a particular particle path line downstream of an unsteady shock wave. Consider the pressure (1) and density (3) equations. These each involve the combination of terms

$$\frac{j}{R_s - x}\rho w^2 (U - w) + \rho w \frac{\mathrm{d}U}{\mathrm{d}t} - \rho w \frac{\partial w}{\partial t} + \frac{\partial P}{\partial t} \,. \tag{10}$$

At the shock front, these terms are identical to corresponding terms in the shock change equation. The magnitude of the curvature term at the shock front is therefore

$$\frac{j}{R-x}\rho w^2(U-w) = \kappa_s \rho_2 w_2^2 \mathrm{u}_2 \text{ at } x = 0 \text{ and } t = t_0\,, \tag{11}$$

where t_o is the instant of time when the fluid element passes through the shock and the subscript 2 indicates the postshock value. The magnitude of the sum of the unsteady terms is

$$\rho w \frac{\mathrm{d}U}{\mathrm{d}t} - \rho w \frac{\partial w}{\partial t} + \frac{\partial P}{\partial t} = \rho_1 a_1^2 f_s \frac{\mathrm{d}M_s}{\mathrm{d}t} \text{ at } x = 0 \text{ and } t = t_0\,. \tag{12}$$

We seek models of each of these terms - models that only depend on time or location on a path line in order to integrate (1) along the path. The location on a path line is implicitly given by integration of the relative velocity

$$\frac{\mathrm{d}x}{\mathrm{d}t} = w \quad \text{and} \quad \frac{\mathrm{d}r}{\mathrm{d}t} = U(t) - w(t;t_0) = \mathrm{u}(t;t_0) \tag{13}$$

to obtain path lines labeled by the time t_0 when the fluid element crosses the shock front

$$x(t;t_0) = \int_{t_0}^{t} w(t';t_0)\,\mathrm{d}t' \quad \text{and} \quad r(t;t_0) = \int_{t_0}^{t} \mathrm{u}(t';t_0)\,\mathrm{d}t' + R_s(t_0)\,. \tag{14}$$

Computing density and flow speed on a path line can be accomplished using relationship developed from the exact path line equations

$$\frac{\mathrm{D}\rho}{\mathrm{D}t} = \rho\left[\frac{1}{\rho a^2}\frac{\mathrm{D}P}{\mathrm{D}t} - \dot{\sigma}\right]\,, \tag{15}$$

$$\frac{\mathrm{D}w}{\mathrm{D}t} = -\frac{1}{\rho w}\left[\frac{\mathrm{D}P}{\mathrm{D}t} - \frac{\partial P}{\partial t}\right] + \frac{\mathrm{d}U}{\mathrm{d}t}\,, \tag{16}$$

and an approximation for either the substantial derivative of density

$$\eta\frac{\mathrm{D}\rho}{\mathrm{D}t} = -\rho\dot{\sigma} + \frac{1}{a^2}\left[\rho w^2 \mathrm{u}\kappa + \rho w\frac{\partial \mathrm{u}}{\partial t} + \frac{\partial P}{\partial t}\right] \tag{17}$$

or pressure

$$\eta\frac{\mathrm{D}P}{\mathrm{D}t} = -\rho w^2\dot{\sigma} + \rho w^2 \mathrm{u}\kappa + \rho w\frac{\partial \mathrm{u}}{\partial t} + \frac{\partial P}{\partial t}\,. \tag{18}$$

The effects of transverse divergence can be approximated by an emprical effective curvature function $\kappa(t)$. For a one-dimensional blast wave and a thin reaction zone

$$\frac{j}{R_s - x} \to \frac{j}{R_s} = \kappa \,. \tag{19}$$

The unsteady terms are more challenging to estimate. One approach, motivated by the shock change relations, is to consider these terms as due to effective shock decay rate and equal to the values at the shock front

$$\rho w \frac{\partial \mathrm{u}}{\partial t} + \frac{\partial P}{\partial t} \to \rho_1 a_1 f \frac{\mathrm{d}U}{\mathrm{d}t} \,. \tag{20}$$

A similar approximation can be proposed for the unsteady pressure term in the w equation

$$\frac{1}{\rho w}\frac{\partial P}{\partial t} + \frac{\mathrm{d}U}{\mathrm{d}t} \to \left[1 + \frac{1}{\rho_1 U}\left(\frac{\partial P}{\partial U}\right)_{\mathcal{H}}\right]\frac{\mathrm{d}U}{\mathrm{d}t} \,, \tag{21}$$

using the nondimensional function

$$g = \left[1 + \frac{1}{\rho_1 U}\left(\frac{\partial P}{\partial U}\right)_{\mathcal{H}}\right] . \tag{22}$$

For perfect gases, this function is independent of shock speed and depends only on the ratio of specific heats

$$g = \frac{\gamma + 5}{\gamma + 1} \qquad 3 \geq g \geq 2.5 \quad \text{for} \quad 1 \leq \gamma \leq 5/3 \,. \tag{23}$$

Critical evaluation of the approximations (19) and (20) requires analyzing direct numerical simulations. This is the approach taken by Eckett et al. (2000), Arienti and Shepherd (2005).

2.1 Temperature Model

The path line energy balance equation can be used to develop an equation for temperature that is more convenient for further simplifications. One version of the balance equation is

$$\frac{\mathrm{D}h}{\mathrm{D}t} = \frac{1}{\rho}\frac{\mathrm{D}P}{\mathrm{D}t} \,. \tag{24}$$

Expanding the mixture enthalpy and distributing the differentiation, we obtain

$$c_p \frac{\mathrm{D}T}{\mathrm{D}t} = -\sum_k h_k \frac{\mathrm{D}Y_k}{\mathrm{D}t} + \frac{1}{\rho}\frac{\mathrm{D}P}{\mathrm{D}t}\,. \tag{25}$$

To complete the model, we need an estimate of the substantial derivative of pressure. The exact value is given by (1) but as pointed out previously, absent a detailed simulation of the flow field, it is necessary to estimate the unknown terms. A possible approach is to use (19) and (20) and assume these terms are constant through the reaction zone.

$$\frac{\mathrm{D}P}{\mathrm{D}t} \approx \left.\frac{\mathrm{D}P}{\mathrm{D}t}\right|_{\mathcal{S}} = \frac{1}{\eta}\left[\rho w \left(\frac{\mathrm{d}u}{\mathrm{d}t}\right)_{\mathcal{S}} + \left(\frac{\mathrm{d}P}{\mathrm{d}t}\right)_{\mathcal{S}} + \rho w^2 \mathrm{u}\kappa\right]_{\mathcal{S}} \tag{26}$$

where the contribution of thermicity $\dot{\sigma}$ is neglected at the shock front. An equivalent approach is to use the energy equation in the form

$$\frac{\mathrm{D}e}{\mathrm{D}t} = \frac{P}{\rho^2}\frac{\mathrm{D}\rho}{\mathrm{D}t}\,, \tag{27}$$

$$c_v \frac{\mathrm{D}T}{\mathrm{D}t} = -\sum_k e_k \frac{\mathrm{D}Y_k}{\mathrm{D}t} + RT\frac{1}{\rho}\frac{\mathrm{D}\rho}{\mathrm{D}t}\,, \tag{28}$$

and the shock change relations to estimate the substantial derivative of density

$$\frac{1}{\rho}\frac{\mathrm{D}\rho}{\mathrm{D}t} \approx \frac{1}{\rho}\left.\frac{\mathrm{D}\rho}{\mathrm{D}t}\right|_{\mathcal{S}} = \frac{1}{\rho a^2 \eta}\left[\rho w \left(\frac{\mathrm{du}}{\mathrm{d}t}\right)_{\mathcal{S}} + \left(\frac{\mathrm{d}P}{\mathrm{d}t}\right)_{\mathcal{S}} + \rho w^2 \mathrm{u}\kappa\right]_{\mathcal{S}} \tag{29}$$

or in terms of shock acceleration

$$\frac{1}{\rho}\frac{\mathrm{D}\rho}{\mathrm{D}t} \approx \frac{1}{\eta}\left[\frac{\rho_1 a_1}{\rho a^2} f \frac{\mathrm{d}U}{\mathrm{d}t} + \frac{w^2}{a^2}\mathrm{u}\kappa\right]_{\mathcal{S}} \tag{30}$$

Note that for decaying shock waves with $\kappa > 0$, the contribution of transverse divergence due to wave curvature is positive and that of unsteadiness is negative. The approximate evoluation equation for temperature is

$$\frac{\mathrm{D}T}{\mathrm{D}t} = -\frac{1}{c_v}\sum_k e_k \frac{\mathrm{D}Y_k}{\mathrm{D}t} + \frac{R}{c_v}\frac{T}{\eta}\left[\frac{\rho_1 a_1}{\rho a^2} f \frac{\mathrm{d}U}{\mathrm{d}t} + \frac{w^2}{a^2}\mathrm{u}\kappa\right]_{\mathcal{S}}\,. \tag{31}$$

We can explicitly identify three separate constributions to temperature change

$$\frac{\mathrm{D}T}{\mathrm{D}t} = \underbrace{-\frac{1}{c_v}\sum_k e_k \frac{\mathrm{D}Y_k}{\mathrm{D}t}}_{\text{chemical}} \quad \underbrace{+\frac{T}{\eta}\frac{R}{c_v}\frac{\rho_1 a_1}{\rho a^2} f \frac{\mathrm{d}U}{\mathrm{d}t}}_{\text{unsteady}} \quad \underbrace{+\frac{T}{\eta}\frac{R}{c_v}\frac{w^2}{a^2}\mathrm{u}\kappa}_{\text{curvature}} . \tag{32}$$

The coefficients of the unsteady and curvature terms are positive so that the sign of these terms depends on the sign of the acceleration and curvature. The chemical term in exothermic reactions has a large positive contribution during the important energy-release phase of the reactions. A key issue in unsteady shock waves such as observed in initiation or propagation of detonations, is the potential for competition between unsteadiness and chemical reaction if the wave is decaying, $\mathrm{d}U/\mathrm{t} < 0$. This competition is responsible to the quenching of reaction behind decaying shock waves and the basis of the *critical decay rate* model proposed by Eckett et al. (2000).

2.2 Shock Change Relations with Uniform Curvature

Modeling the flow as one-dimensional in a planar ($j = 0$), cylindrical ($j = 1$), or spherical ($j = 2$) coordinate system, the conservation of mass equation can be written as in terms of a radial coordinate r

$$\frac{1}{\rho}\frac{\mathrm{D}\rho}{\mathrm{D}t} = -\frac{\partial \mathrm{u}}{\partial r} - \frac{j}{r}\mathrm{u} \tag{33}$$

For a shock wave of radius R_s moving with a speed $U = dR_s/dt$, the methodology used for the planar shock change relations can be extended to a curved wave. For the case of a uniform, stationary upstream the following versions of the shock change relation can be derived

$$\rho w\left(\frac{\mathrm{d}u}{\mathrm{d}t}\right)_{\mathcal{S}} + \left(\frac{\mathrm{d}P}{\mathrm{d}t}\right)_{\mathcal{S}} = \rho a^2\left(-\eta\frac{\partial u}{\partial r} + \dot{\sigma} - \frac{j\,\mathrm{u}}{R_s}\right) \tag{34}$$

$$\rho w\left(\frac{\mathrm{d}u}{\mathrm{d}t}\right)_{\mathcal{S}} + \left(\frac{\mathrm{d}P}{\mathrm{d}t}\right)_{\mathcal{S}} = \rho a^2\left(\eta\frac{1}{\rho}\frac{\mathrm{D}\rho}{\mathrm{D}t} + \dot{\sigma} - \frac{w^2}{a^2}\frac{j\,\mathrm{u}}{R_s}\right) \tag{35}$$

$$\rho w\left(\frac{\mathrm{d}u}{\mathrm{d}t}\right)_{\mathcal{S}} + \left(\frac{\mathrm{d}P}{\mathrm{d}t}\right)_{\mathcal{S}} = \rho a^2\left(\eta\frac{1}{\rho a^2}\frac{\mathrm{D}P}{\mathrm{D}t} + \frac{w^2}{a^2}\dot{\sigma} - \frac{w^2}{a^2}\frac{j\,\mathrm{u}}{R_s}\right) \tag{36}$$

Using the thermodynamic transformations and shock jump conditions, the left-hand side can be written in terms of the derivatives on the Hugoniot and the shock acceleration

$$\rho w\left(\frac{\mathrm{d}u}{\mathrm{d}t}\right)_{\mathcal{S}} + \left(\frac{\mathrm{d}P}{\mathrm{d}t}\right)_{\mathcal{S}} = \left[1 + \rho_1 U\left(\frac{\mathrm{d}u}{\mathrm{d}P}\right)_{\mathcal{H}}\right]\left(\frac{\mathrm{d}P}{\mathrm{d}U}\right)_{\mathcal{H}}\frac{\mathrm{d}U}{\mathrm{d}t} \tag{37}$$

The coefficient multiplying shock acceleration can written in terms of a nondimensional function f

$$f = \frac{1}{\rho_1 a_1}\left[1 + \rho_1 U \left(\frac{\mathrm{du}}{\mathrm{d}P}\right)_{\mathcal{H}}\right]\left(\frac{\mathrm{d}P}{\mathrm{d}U}\right)_{\mathcal{H}}, \tag{38}$$

and the left-hand side of (36) can be written as

$$\rho_1 U \left(\frac{\mathrm{du}}{\mathrm{d}t}\right)_{\mathcal{S}} + \left(\frac{\mathrm{d}P}{\mathrm{d}t}\right)_{\mathcal{S}} = \rho_1 a_1 f \frac{\mathrm{d}U}{\mathrm{d}t}\,. \tag{39}$$

For a perfect gas, the function f can be given analytically in terms of shock Mach number $M_s = U/a_1$

$$f = \frac{4}{\gamma+1}\left[\frac{3}{2}M_s + \frac{1}{2M_s}\right] \tag{40}$$

Expressing the unsteady contributions in terms of shock acceleration, the the substantial derivative of pressure at the shock front can be expressed as

$$\eta \frac{\mathrm{D}P}{\mathrm{D}t} = \underbrace{-\rho w^2 \dot{\sigma}}_{\text{chemical}} \quad \underbrace{+\rho w^2 \frac{\mathrm{u}\, j}{R_s}}_{\text{curvature}} \quad \underbrace{+\rho_1 a_1 f \frac{\mathrm{d}U}{\mathrm{d}t}}_{\text{unsteady}}\,. \tag{41}$$

(42)

The chemical term represents the exchange of energy between molecular process and the flow. This contribution is identical to that obtained in the previous analyses of reaction zones behind steady shock waves. The curvature term is more properly described as a transverse divergence contribution and can be generalized as discussed below. The unsteady terms are all proportional to the shock acceleration $\mathrm{d}U/\mathrm{d}t$. The sign and magnitude of each term depends on the specific details of chemistry and shock wave configuration. The main distinctions are between exothermic $\dot{\sigma} < 0$ and endothermic $\dot{\sigma} > 0$ reactions at the shock front, diverging ($R_s > 0$) and converging ($R_s < 0$) shock waves, accelerating ($\mathrm{d}U/\mathrm{d}t > 0$) and decelerating ($\mathrm{d}U/\mathrm{d}t < 0$) shocks.

The interpretation of the curvature term is facilitated by considering quasi-steady flow behind a propagating curved shock, which gave the relationship of stream tube area A change immediately behind the front to the shock radius R_s. In the shock-fixed coordinate system, this correspondence is

$$\frac{j\,\mathrm{u}}{R_s} = w \frac{1}{A}\frac{\mathrm{d}A}{\mathrm{d}x} \tag{43}$$

In an unsteady flow, there are no well-defined stream tubes so it is more appropriate to refer to the curvature term as being associaed with the transverse component of flow divergence. The kinematics of fluid motions links the flow divergence to the density or volume rate of change through the continuity equation

$$\frac{1}{\rho}\frac{\mathrm{D}\rho}{\mathrm{D}t} = -\frac{1}{v}\frac{\mathrm{D}v}{\mathrm{D}t} = -\nabla\cdot\mathbf{u} \tag{44}$$

The divergence can be divided into components parallel and transverse to the path line. In cartesian coordinates, the divergence is

$$\nabla\cdot\mathbf{u} = \underbrace{\frac{\partial u}{\partial x}}_{\text{parallel to path}} + \underbrace{\frac{\partial v}{\partial y}+\frac{\partial w}{\partial z}}_{\text{transverse to path}} \tag{45}$$

In radially symmetric coordinates attached to the shock front, the transverse component is

$$\underbrace{\nabla\cdot\mathbf{u}}_{\text{transverse to path}} = \frac{j\ \mathrm{u}}{R_s - x}\,. \tag{46}$$

3 Application to Cellular Structure Modeling

We have used the critical decay rate model to examine the flow behind the leading shock waves for two cases (Fig. 1 and Fig. 2) examined in the NCF experiments. The initial conditions and nominal CJ conditions are given in Table 1.

The reaction zone structure and associated length and time scales depend strongly on the shock speed which determines the postshock temperature and pressure, Fig. 1. The induction time dependence on temperature displays an Arrhenius behavior, $t_i \propto \exp(-E_a/\tilde{R}T)$, with an effective activation energy E_a varying from 33 to 47 kcal·mol^{-1} with increasing shock speed. The effective activation energy E_a is an important parameter in the analytical model for the critical decay rate in reduced form, $\Theta = E_a/\tilde{R}T$, shown in Fig. 2

Using these parameters, the magnitude of the thermodynamic derivatives, unsteady and curvature terms in the model temperature equation can be evaluated and used to compute the density time derivative at the shock

Table 1: Reaction parameters for CH_4-$2O_2$-$2.5N_2$ mixture.

P_0	18.8	kPa
T_0	295	K
U_{CJ}	2016.8	$\mathrm{m} \cdot \mathrm{s}^{-1}$
P_{vN}	751.5	kPa
T_{vN}	1663.5	K
ZND reaction		
t_i $(\dot{\sigma}_{max})$	23.4	μs
t_e $(\dot{\sigma}_{1/2})$	0.261	μs
Δ_i $(\dot{\sigma}_{max})$	0.888	mm
Δ_e $(\dot{\sigma}_{1/2})$	0.157	mm
Constant-pressure reaction		
t_i $(\dot{T}_{max})$	26.4	μs
t_e $(\dot{T}_{1/2})$	0.231	μs
E_a	45.1	kcal$\cdot$ mol^{-1}
Θ	13.6	-
Constant-volume reaction		
t_i $(\dot{T}_{max})$	24.4	μs

front from the shock change equation (30). Using a detailed reaction mechanism and realistic thermochemistry `gri30_highT`, the Cantera software and Shock and Detonation Toolbox was used to evaluate all quantities and perform numerical integration of the model temperature equation.

The two thermodynamic properties f and g were computed using finite differences. As expected from the perfect gas expressions, there is a modest dependence of f on shock speed and essentially no dependence of g on shock speed. The effective value of $\gamma = c_p/c_v$ based on frozen postshock properties has a modest dependence on shock speed, Fig. 3.

In order to apply the model to a decaying shock we will estimate the volume expansion rate along a path line using the measured shock decay rate and curvature, assuming these quantities have constant values equal to

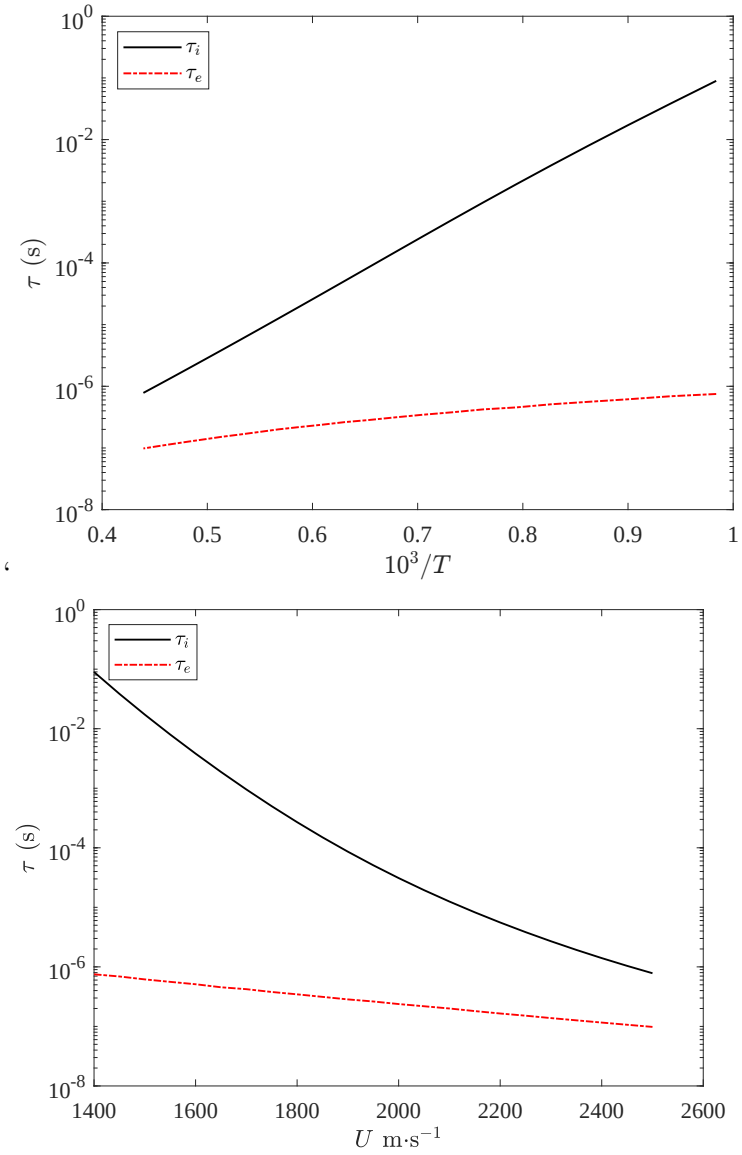

Figure 1: Time scales computed for constant pressure reaction behind shock waves in the CH_4-$2O_2$-$2.5N_2$ mixture.

those at the shock front. We can write the temperature equation on the

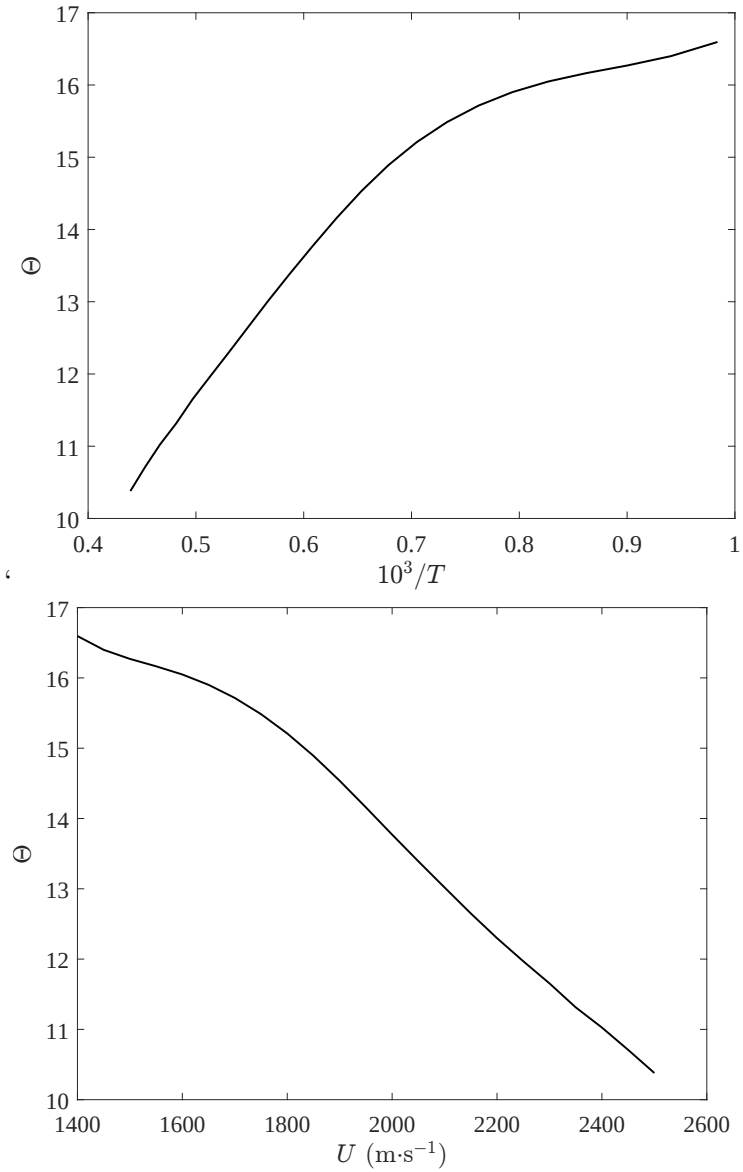

Figure 2: Effective activation energy for constant pressure reaction behind shock waves in the CH_4-$2O_2$-$2.5N_2$ mixture.

path line as

$$\frac{\mathrm{D}T}{\mathrm{D}t} = -\frac{1}{c_v}\sum_k e_k \frac{\mathrm{D}Y_k}{\mathrm{D}t} + T\frac{R}{c_v}\frac{1}{\rho}\frac{\mathrm{D}\rho}{\mathrm{D}t}\,, \tag{47}$$

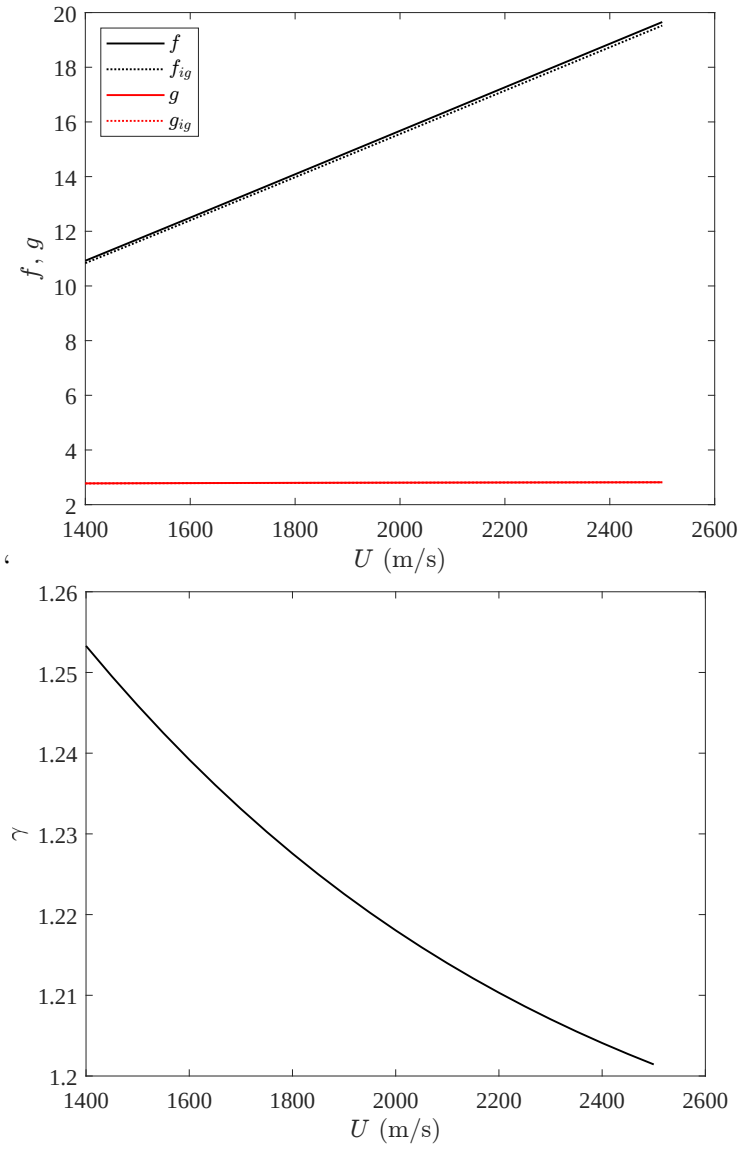

Figure 3: Shock adiabat derivatives and effective specific heat ratio γ for for CH_4-$2O_2$-$2.5N_2$ mixture mixture.

where the rate of change of density on the path line is given by

$$\frac{\mathrm{D}\rho}{\mathrm{D}t} = -\frac{\rho}{\tau_v}\,, \tag{48}$$

and the time constant τ_v is determined from the unsteadiness and curvature of the shock at the time the path line passes through the shock.

$$\frac{1}{\tau_v} = -\frac{1}{\eta}\left[\frac{\rho_1 a_1}{\rho a^2} f \frac{\mathrm{d}U}{\mathrm{d}t} + \frac{w^2}{a^2}\mathrm{u}\kappa\right]_{\mathcal{S}} . \tag{49}$$

The variation of species concentrations along the path line is determined by the net reaction rate Ω_i and the network of reactions in the mechanism

$$\frac{\mathrm{D}Y_k}{\mathrm{D}t} = \Omega_k . \tag{50}$$

This model has obvious deficiencies, most notably that it does not account for the variation of shock unsteadiness and curvature with time and the propagation of these effects into the flow behind the leading shock front. For certain situations, as discussed in Eckett et al. (2000), these assumptions can be justified but in general these need to be examined on a case by case basis. The expression for the time constant can be simplified and written as

$$\frac{1}{\tau_v} = -A(U)\frac{\mathrm{d}M_s}{\mathrm{d}t} - B(U)a_1\kappa \tag{51}$$

where $M = U/a_1$ is the shock Mach number, and the nondimensional coefficients A and B are a function of shock speed U for a given mixture composition and initial conditions.

$$A = \frac{1}{\eta}\frac{\rho_1 a_1^2}{\rho a^2} f \tag{52}$$

$$B = \frac{1}{\eta}\frac{w^2}{a^2}\frac{\mathrm{u}}{a_1} \tag{53}$$

The values bracketing the velocities considered (1600 to 2600 $\mathrm{m{\cdot}s^{-1}}$) in the NCF study are shown in Fig. 4. Analytical approximate expressions for these coefficients can be obtained from the strong shock limits of the perfect gas shock jump conditions.

$$\lim_{M_s\to\infty} A = \frac{1}{M_s}\frac{6}{\gamma+1} = A_{ss} \tag{54}$$

$$\lim_{M_s\to\infty} B = 2M_s\frac{\gamma-1}{(\gamma+1)^2} = B_{ss} \tag{55}$$

The approximate values have the same qualitative dependence on shock speed as the values based on thermodynamics derivatives of the actual shock adiabat but the values are lower by 15% in the case of A and 25% in the case of B.

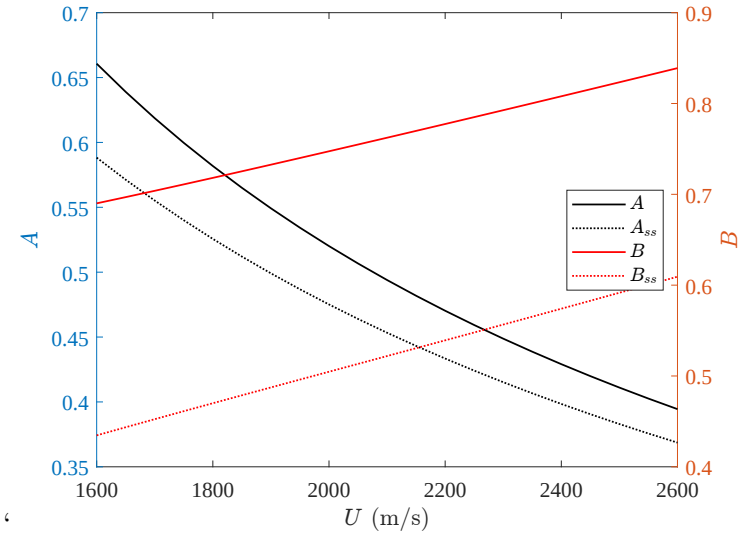

Figure 4: Coefficients A and B used to compute the expansion time scale in the CH_4-$2O_2$-$2.5N_2$ mixture.

4 Figure 4 Analysis

The estimated lead shock speed and curvature for this case are shown in Fig. 5 The curvature and shock speed data are sufficiently smooth that these

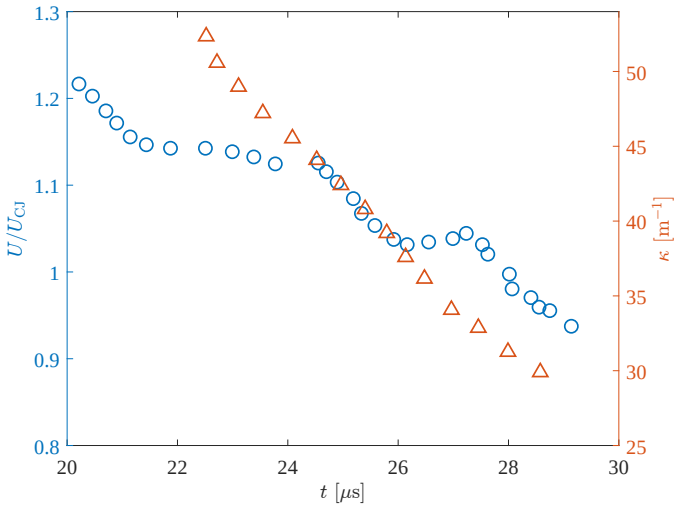

Figure 5: Lead shock speed and curvature for Fig. 4 of the main text.

can be used directly in evaluating the model terms. However, we also need to estimate the shock acceleration. Given the discrete nature of the data, it is necessary to make an estimate using finite differences. We are, of course, in a "state of sin" in attempting to extract derivatives from sparse and noisy data. Plowing ahead, we have used the time-honored dodge of applying a filtering technique to reduce the noise. We interpolated the original data onto 100 points and then used a third-order Savitzky-Golay filter with a seven-point frame[1] to make the estimate shown in Fig. 6.

Given the noisy and unreliable nature of the computed acceleration (shown as open symbols for selected paths on Fig. 6), we opted to use the average acceleration of -6.2×10^7 m · s^{-2}, shown as the horizontal line in the figure. This is a crude approximation and as a consequence, the results of the modeling only give a qualitative indication of the effects of unsteadiness. The expansion time scale τ_v and the individual contributions due to unsteadiness and curvature are shown in Fig. 7. The contribution of shock

[1] This operation was performed in MATLAB using the `interp1` function with the `pchip` option and the `sgolay` filter.

unsteadiness is a factor of 5 to 10 times larger than the curvature throughout the duration analyzed. This is consistent with findings of Eckett et al. (2000) who observed that during spherical blast wave initiation of detonation, the unsteadiness clearly dominated the effect of curvature.

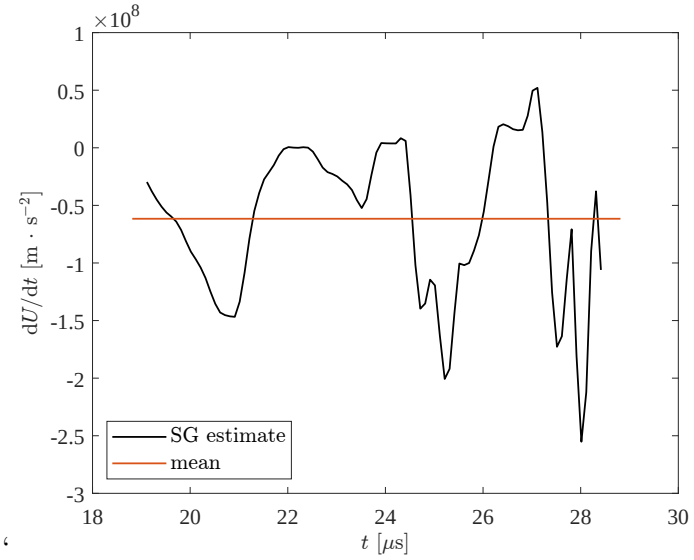

Figure 6: Acceleration of lead shock of Fig. 4 estimated using the polynomial fit to the data.

The approximation reaction zone equations (47-50) were integrated for each path and the results are shown in Fig. 8. As the shock decays, the reaction time increases due to the decrease of post shock temperature and reaction rate with decreasing shock speed. An additional increase in reaction time occurs due to the competition between volume expansion and chemical reaction, further increasing the reaction time as expansion becomes more competitive with reaction in the latter portions of the decay process. Ultimately, this results in the quenching of the reaction and disappearance of the exothermic reaction temperature rise for path lines later than number 7.

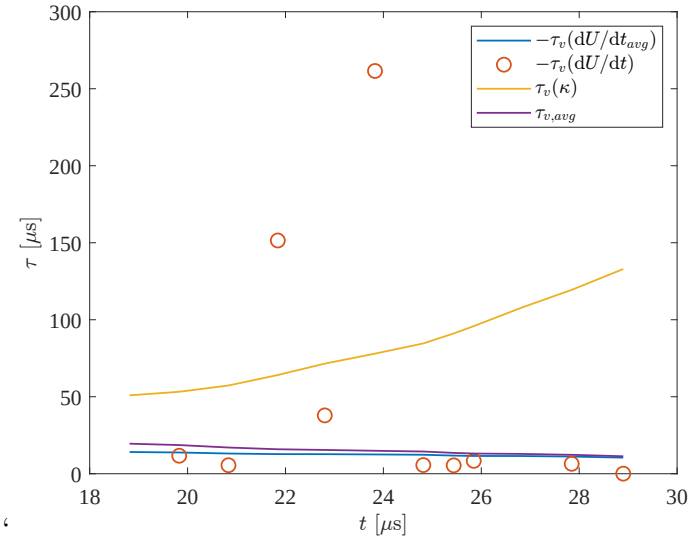

Figure 7: Expansion time scales τ_v for the path lines of Fig. 4 in the main text. For clarity, extreme values of the time scales for small values of the acceleration are omitted.

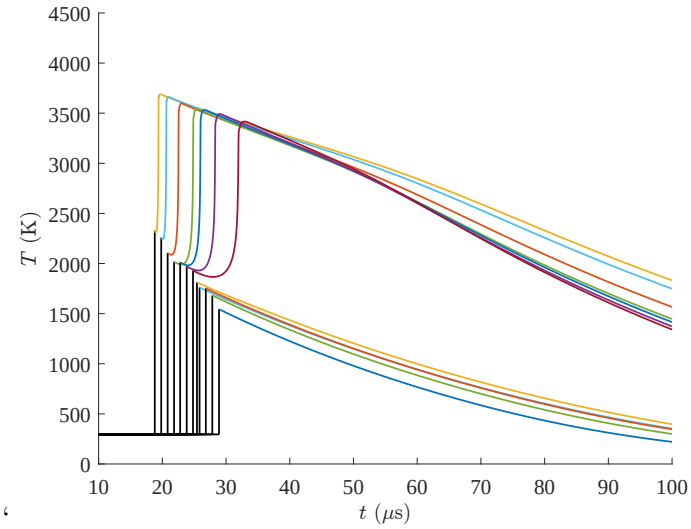

Figure 8: Results of modeling unsteady reaction along the path lines of Fig. 4 in the main text.

Associated with each path line is an induction time t_i (defined as the time to maximum temperature gradient) and a critical decay time τ_v^* that results in quenching of the reaction for a decay time $\tau_v \leq \tau_v^*$. The critical decay time can be detemined by a parameter study, varying τ_v for a given path line until quenching is observed. An example of this computation for path 8, which is close to the critical condition for quenching is shown in Fig. 9.

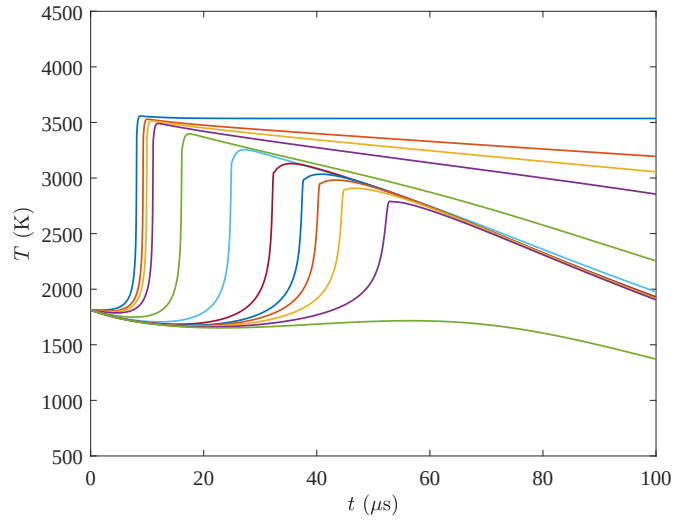

Figure 9: Results of parametric study of the effect of τ_v for reaction along the path line 8 of Fig. 4 in the main text.

The critical parameters associated with each path line are given in Table 2

The critical decay time can be visualized by plotting the induction time as a function of decay rate, shown for path 8 in Fig. 10. The critical decay time corresponds to the vertical asymptote corresponding to $t_i \to \infty$ as $\tau_v \to \tau_v^*$. The qualitative dependence of the reaction time t_i on the expansion time τ_v is consistent with the analytical model derived by Eckett et al. (2000) and described in more detail by Shepherd (2020).

$$t_i = -\frac{t_i^\circ}{\alpha} \ln(1-\alpha)\,, \quad \alpha = \frac{\tau_v^*}{\tau_v}\,. \tag{56}$$

where t_i° is the induction time as defined by the singularity in the asymptotic theory (high activation energy expansion) of ignition of a constant volume ($\tau_v \to \infty$) explosion. The critical value of the expansion time scale, τ_v^*, is

Table 2: Reaction zone and critical decay parameters for Fig. 4.

Path	$U/U_{\rm CJ}$	t_i (μs)	τ_v^* (μs)	τ_v (μs)
1	1.260	0.621	1.18	19.3
2	1.233	0.844	1.61	18.4
3	1.176	1.69	3.63	16.9
4	1.143	2.61	5.74	15.7
5	1.140	2.71	6.20	15.3
6	1.125	3.37	7.86	14.8
7	1.108	4.29	10.0	14.3
8	1.062	8.95	23.35	13.4
9	1.041	12.7	34.9	13.0
10	1.037	13.5	37.7	12.8
11	1.007	23.6	68.8	12.2
12	0.948	76.5	252	11.3

given by the asymptotic model in terms of the reduced activation energy $\Theta = E_a/\tilde{R}T$, where T is the postshock temperature.

$$\tau_v^* = (\gamma - 1)\Theta t_i^\circ \tag{57}$$

For path line 8, $\Theta = 12.6$, $\gamma = 1.215$, $t_i^\circ = 9.5$ μs and the predicted value of the critical expansion time scale is 25.7 μs, about 10% higher the value of 23.35 μs computed using the reaction zone model with a detailed reaction mechanism and realistic thermochemistry.

4.1 Path lines 7 and 8

Path lines 7 and 8 are predicted to bracket the critical decay case. Details of the thermodynamic properties, terms in the energy equation and species are shown in Fig. 11-14. These two path lines illustrate the crossover between reactive and quenched paths. For path 7, the maximum chemical reaction contribution to temperature rate of change is two orders of magnitude larger than the unsteadiness (Fig. 11) and the reaction is not quenched. Rapid energy release occurs at about 32 μs as observed in both the large increase in pressure, consumption of fuel and generation of products, Fig. 12.

For path 8, the maximum chemical reaction contribution to temperature rate of change is one order of magnitude smaller than the unsteadiness

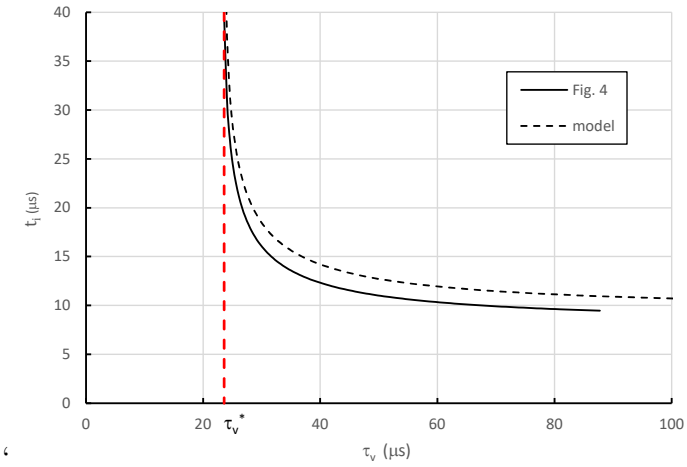

Figure 10: Induction time t_i vs. expansion time τ_v for reaction along the path line 8 of Fig. 4 in the main text and the model of (56).

(Fig. 13) and the reaction is quenched. An energy release transient is not observed, the pressure decreases with increasing time in an approximately isentropic relationship to volume. There are intermediates and radical species created following the passage of the shock wave but the concentrations are not sufficient to initiate a coupled chain-branching thermal explosion that characterizes the energy release zone observed in reactive path lines like number 7.

The shock speed decreases by only 4% from path 7 to path 8, Table 2. Due to the sensitivity of induction time t_i and critical expansion time τ_v^* to postshock temperature, this variation is sufficient to tip the balance between chemical and unsteady contributions to the temperature rate of change. Note that the shock speed in both cases is greater that the CJ value and the unsteady effect plays an essential role that cannot be accounted for by the classical models of detonation propagation.

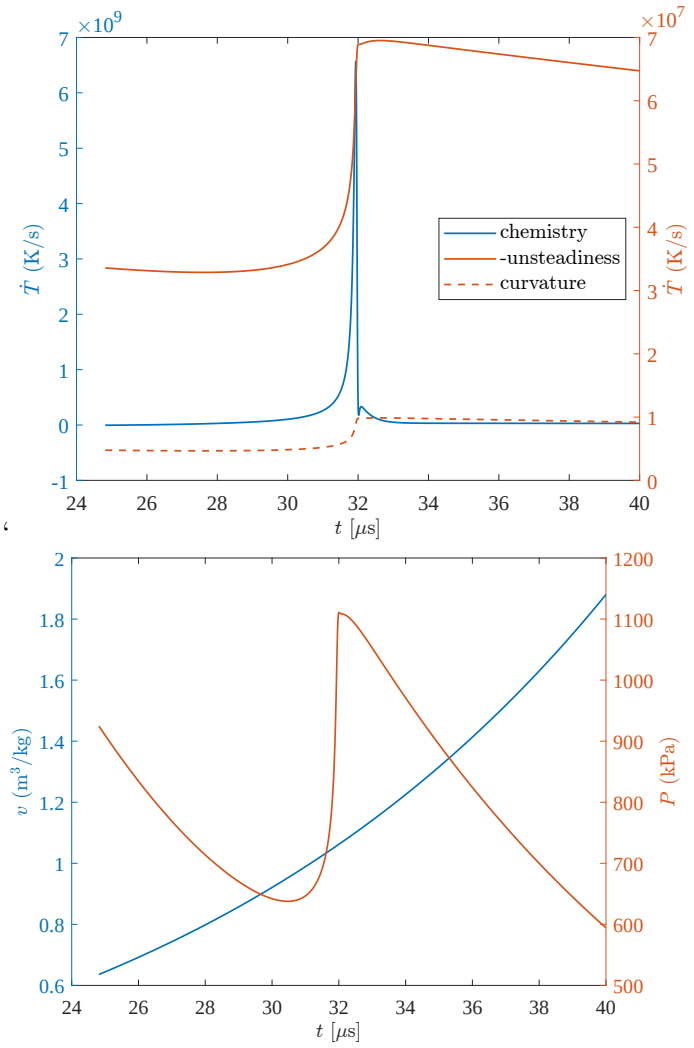

Figure 11: Path 7 energy equation terms (defined in 32), pressure and volume variation in reaction zone.

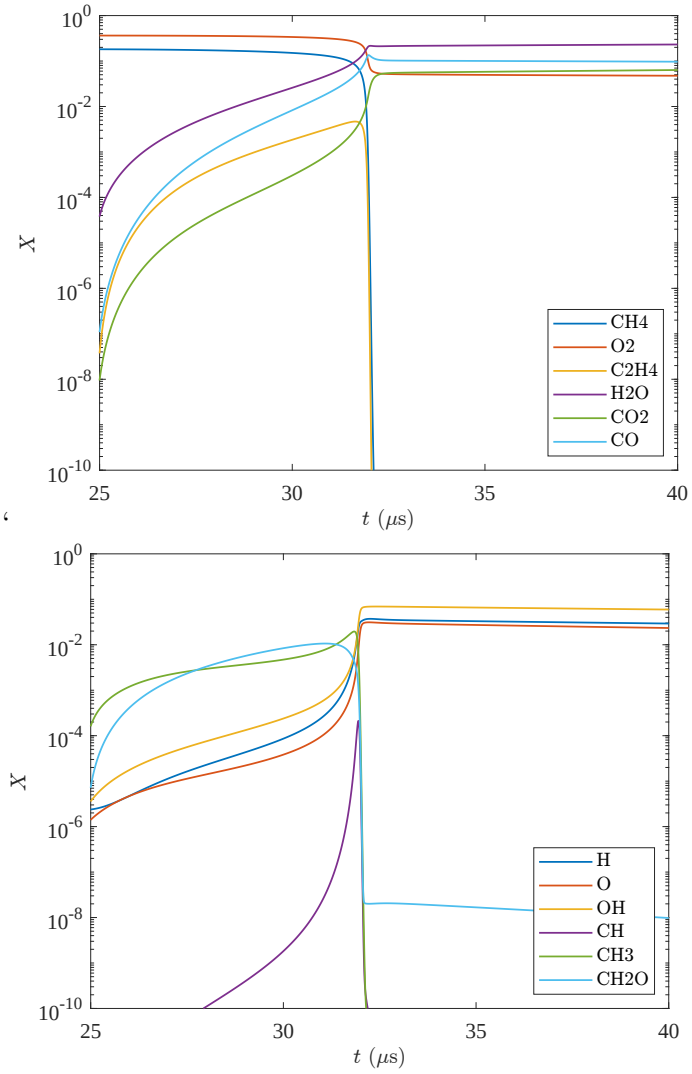

Figure 12: Path 7 major and minor species variation in reaction zone.

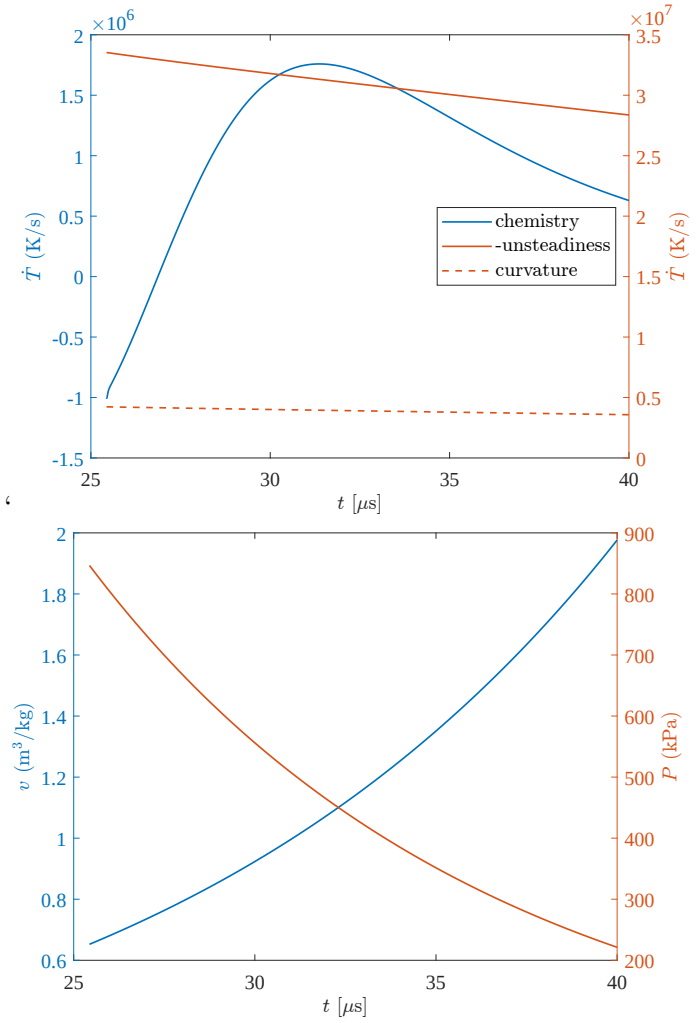

Figure 13: Path 8 energy equation terms, pressure and volume variation in reaction zone.

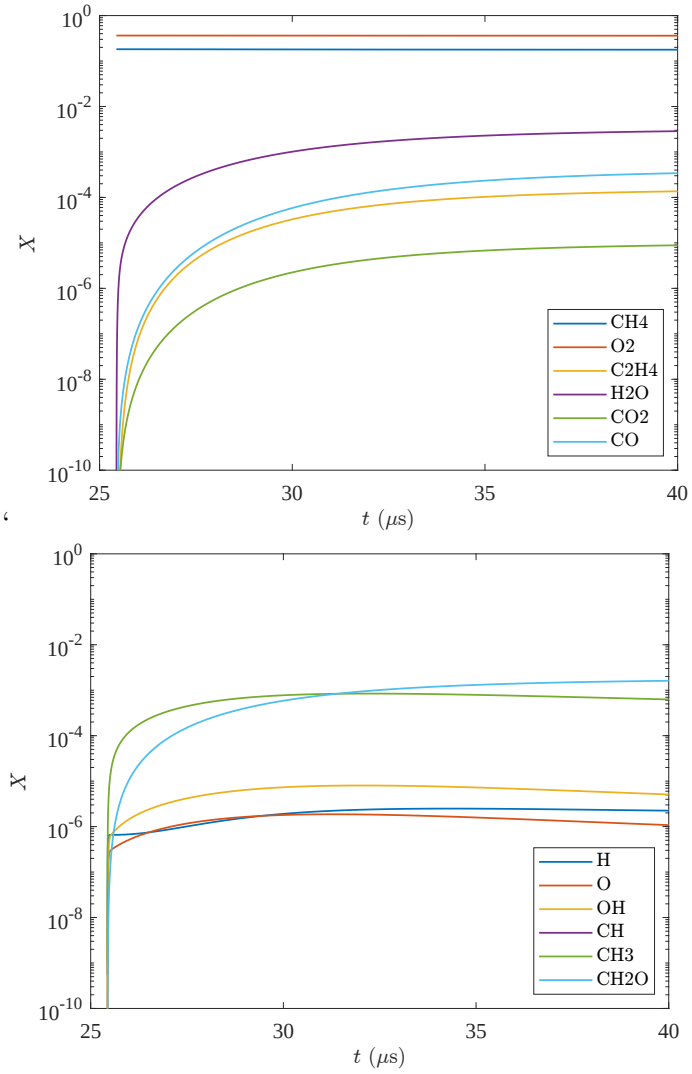

Figure 14: Path 8 major and minor species variation in reaction zone.

5 Figure 5 Analysis

The estimated lead shock speed and curvature for this case are shown in Fig. 15 The most significant difference with the Fig. 4 lead shock is the lower

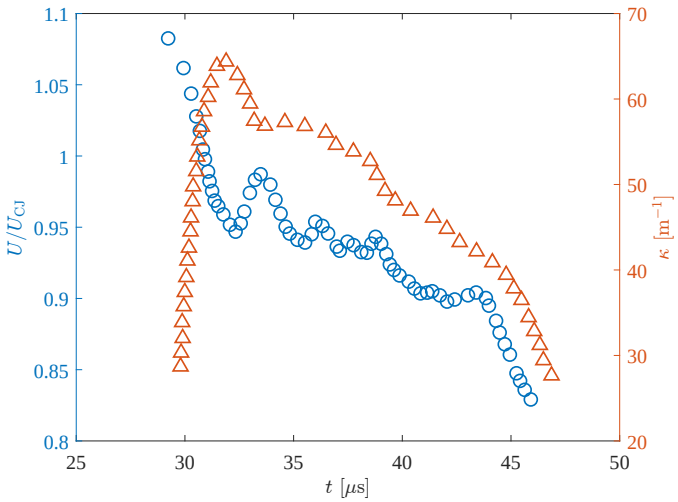

(a) (b)

Figure 15: Shock speed and curvature for path lines shown in Fig. 5 of the main text.

value of the lead shock speed and more rapid decay in the early and late phases of the wave propagation. The lower shock speeds than Fig. 4 result in much longer induction and critical expansion times. The instantaneous acceleration for this case is quite irregular, Fig. 16 and for the purposes of computing the reaction zone the acceleration was modeled with two constant values depending on the time range.

$\mathrm{d}U/\mathrm{d}t_{avg}$	-9.1×10^7 m·s^{-2}	29.2 to 32.3 μs	paths 1-4
$\mathrm{d}U/\mathrm{d}t_{avg}$	-1.6×10^7 m·s^{-2}	32.3 to 45.7 μs	paths 5-7

The critical parameters associated with each path line are given in Table 3. In all cases, the effective volume expansion time τ_v is smaller than the critical decay time τ_v^*, indicating that the reaction will be quenched. This is a consequence primarily of the lower shock speeds which results in much longer induction and critical decay times as compared to the path lines of Fig. 4 in the main text. This is verified by the reaction zone computations shown in Fig. 17. An example of a quenched case is path 1. The

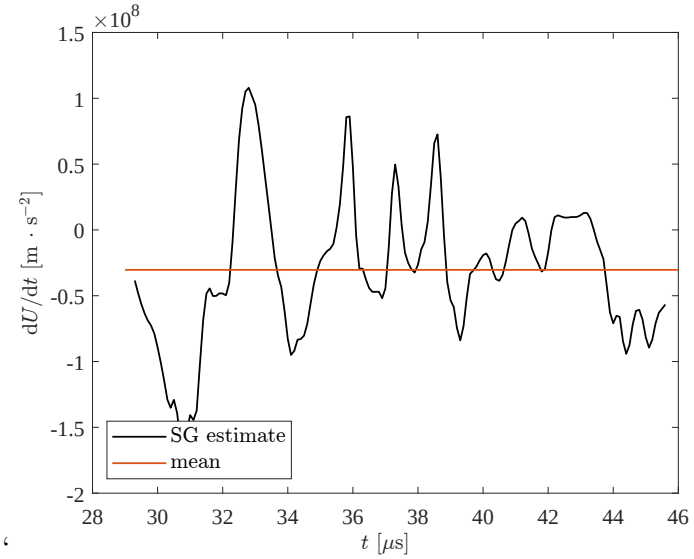

Figure 16: Acceleration of lead shock of Fig. 4 estimated using the polynomial fit to the data.

energy equation terms, pressure and volume dependence on time are shown in Fig. 18. Selected species dependence on time are shown in Fig. 19.

Table 3: Reaction zone and critical decay parameters for Fig. 4.

Path	U/U_{CJ}	t_i (μs)	τ_v^* (μs)	τ_v (μs)
1	1.084	6.18	16.3	7.94
2	1.050	11.0	29.5	8.65
3	0.980	39.3	124	8.30
4	0.950	72.1	242	8.02
5	0.983	36.7	116	105
6	0.969	48.6	157	99.7
7	0.941	88.0	302	90.8

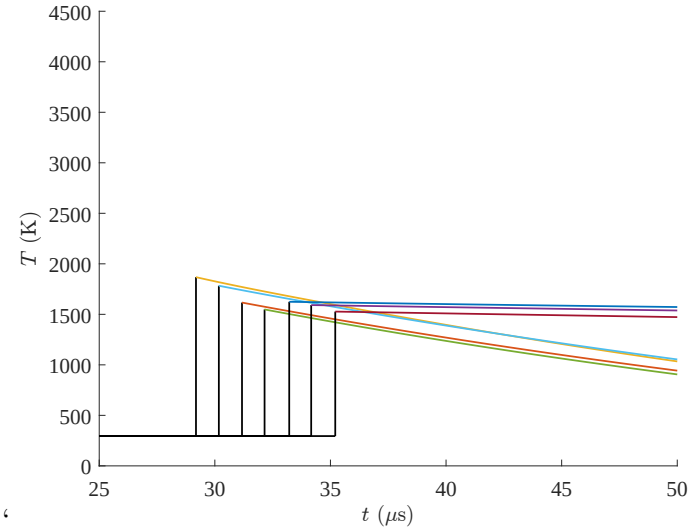

Figure 17: Results of modeling unsteady reaction along the path lines of Fig. 5 in the main text.

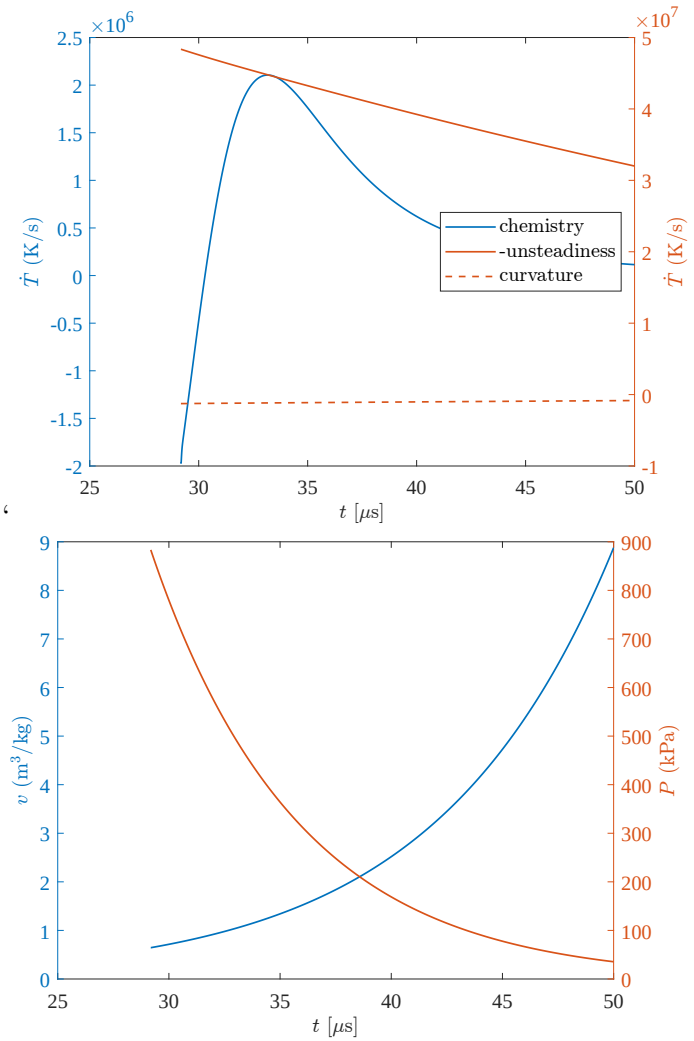

Figure 18: Path 1 energy equation terms (defined in 32), pressure and volume variation in reaction zone.

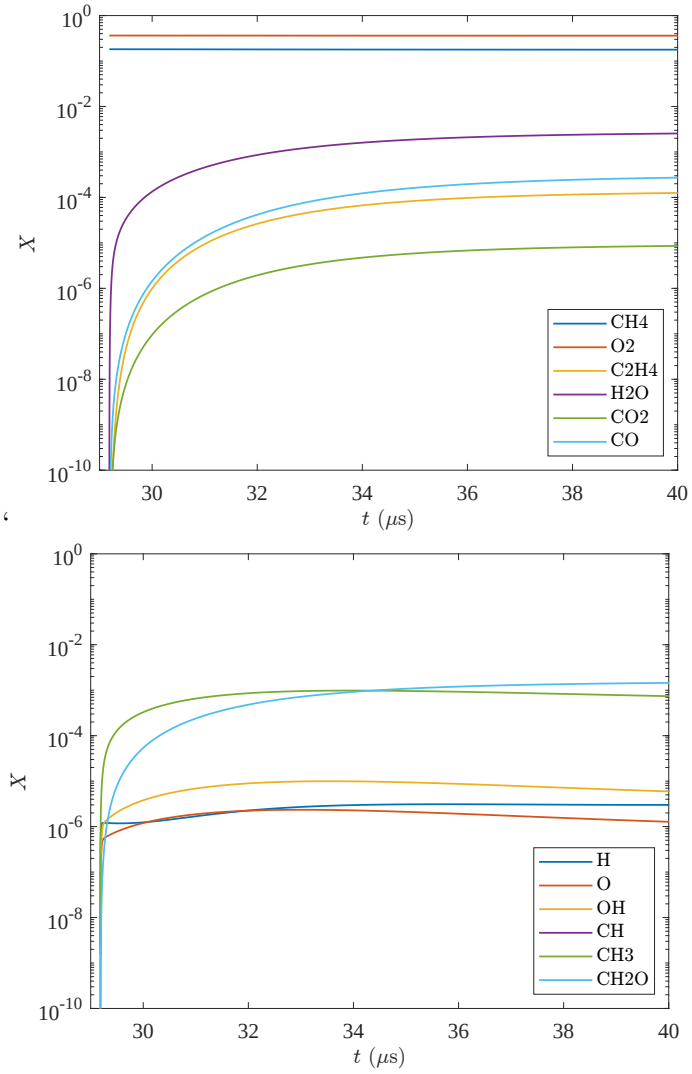

Figure 19: Path 1 major and minor species variation in reaction zone.

6 Summary

The results of the unsteady reaction zone simulations are concisely represented in Fig. 20. Symbols to the left of the critical expansion time scale, τ_v^* are predicted to correspond to path lines with quenched reaction due to effects of shock wave unsteadiness. Consistent with the detailed computations of reaction processes, Fig. 4 cases are predicted to quench between path lines 7 and 8 while all path lines for the Fig. 5 cases are predicted to quench.

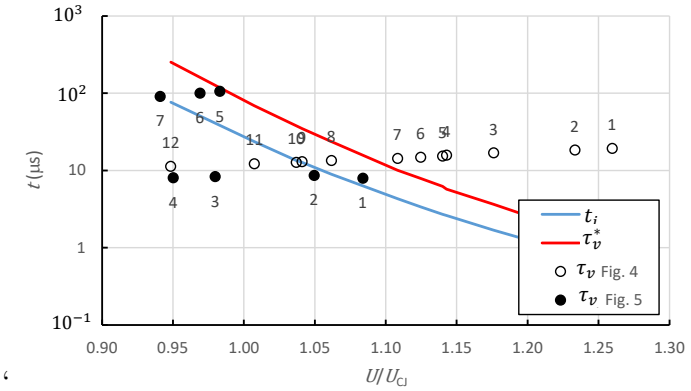

Figure 20: Summary of the CDR study for path lines of Fig. 4 and Fig. 5 in the main text.

We acknowledge that there are significant limitations to our modeling approach, particularly the assumptions that the characteristic time τ_v is constant along path lines. It is also challenging to extract reliable acceleration and shock curvature from discrete experimental data of shock location vs. time. Even using the most advanced diagnostic instruments at our disposal, there are large uncertainties in these values.

Despite the uncertainties, the qualitative results provide significant physical insight and are consistent with the visual observations of reaction zone structure. Our results are also limited to a single mixture composition and it is known Shepherd (2009) that the stability and regularity of cellular structure is a strong function of composition and the coupling to the confining channel. We anticipate that mixtures with more regular cellular patterns will be more amenable to analysis with lower uncertainties.

References

M. Arienti and J. E. Shepherd. A Numerical Study of Detonation Diffraction. *J. Fluid Mech.*, 529:117–146, 2005. (Preprint - see journal for final version http://dx.doi.org/10.1017/S0022112005003319). 4, 8

J. M. Austin, F. Pintgen, and J. E. Shepherd. Lead shock oscillation and decoupling in propagating detonations. In *43nd AIAA Aerospace Sciences Meeting*, pages AIAA 2005–1170, Reno, NV, 2005a. AIAA. 3

J. M. Austin, F. Pintgen, and J. E. Shepherd. Reaction zones in highly unstable detonations. *Proc. Combust. Inst.*, 30(2):1849–1857, January 2005b. 3

E Becker. Chemically Reacting Flows. *Ann. Rev. Fluid Mech.*, 4:155–194, 1972. 4

Kevin Cheevers. *Optical Fibre-based Hydrophone and Critical Ignition in Detonation Cells*. MS Thesis, University of Ottawa, Ottawa, Canada, 2021. 3

Peter J. Chen and Morton E. Gurtin. Growth and Decay of One-Dimensional Shock Waves in Fluids with Internal State Variables. *Physics of Fluids*, 14(6):1091–1094, 1971. 4

S.A. Coronel, J.-C. Veilleux, and J. E. Shepherd. Ignition of Stoichiometric Hydrogen-Oxygen by Water Hammer. *Proceedings of the Combustion Institute*, 38(3):3537–3545, 2020. 3

C. A. Eckett, J. J. Quirk, and and J. E. Shepherd. The role of unsteadiness in direct initiation of gaseous detonations. *Journal of Fluid Mechanics*, 421:147–183, 2000. 2, 3, 4, 6, 8, 10, 17, 20, 22

G. Emanuel. *Shock Wave Dynamics - Derivatives and Related Topics*. CRC Press/Taylor & Francis, Boca Raton, FL, 2013. 4

W. Fickett and W. C. Davis. *Detonation*. University of California Press, Berkerely, CA, 1979. 3, 4

Vadim N. Gamezo, Daniel Desbordes, and Elaine S. Oran. Formation and evolution of two-dimensional cellular detonations. *Combustion and Flame*, 116(1-2):154–165, January 1999a. 3

V.N. Gamezo, D. Desbordes, and E.S. Oran. Two-dimensional reactive flow dynamics in cellular detonation waves. *Shock Waves*, 9(1):11–17, February 1999b. 3

Scott I. Jackson and Mark Short. The influence of the cellular instability on lead shock evolution in weakly unstable detonation. *Combustion and Flame*, 160(10):2260–2274, October 2013. 3

Scott I. Jackson, Carlos Chiquete, and Mark Short. An intrinsic velocity–curvature–acceleration relationship for weakly unstable gaseous detonations. *Proceedings of the Combustion Institute*, 37(3):3601–3607, 2019. 3

J.E. Kennedy and J.W. Nunziato. Shock-wave evolution in a chemically reacting solid. *Journal of the Mechanics and Physics of Solids*, 24(2-3): 107–124, June 1976. 4

J. H. S. Lee. *The Detonation Phenomenon*. Cambridge University Press, New York, NY USA, 2008. 3

E. A. Lundstrom and A. K. Oppenheim. On the influence of non-steadiness on the thickness of the detonation wave. *Proceedings of the Royal Society of London. A. Mathematical and Physical Sciences*, 310(1503):463–478, June 1969. 3

B.M. Maxwell and M.I. Radulescu. Ignition limits of rapidly expanding diffusion layers: Application to unsteady hydrogen jets. *Combustion and Flame*, 158(10):1946–1959, October 2011. 3

J. W. Nunziato and E. K. Walsh. Propagation and Growth of Shock Waves in Inhomogeneous Fluids. *Physics of Fluids*, 15(8):1397–1402, 1972. 4

J. W. Nunziato and E. K. Walsh. Shock-wave propagation in inhomogeneous atmospheres. *Physics of Fluids*, 16(4):482–484, 1973. 4

Jace W. Nunziato. One-dimensional shock waves in a chemically reacting mixture of elastic materials. *The Journal of Chemical Physics*, 58(3): 961–965, February 1973. 4

R L Rabie and Jerry Wackerle. Three-Dimensional Shock-Change Relations for Reactive Fluids. Technical Report LA-7253, Los Alamos Scientific Laboratory, May 1978. 4

M. I. Radulescu. On the shock change equations. *Physics of Fluids*, 32(5): 056106, May 2020. 4

Matei I. Radulescu and Chung K. Law. The transient start of supersonic jets. *Journal of Fluid Mechanics*, 578:331–369, May 2007. 3

Matei I. Radulescu and Brian M. Maxwell. Critical ignition in rapidly expanding self-similar flows. *Physics of Fluids*, 22(6):066101, June 2010. 3

J. E. Shepherd. Detonation in gases. In *Proceedings of the Combustion Institute*, volume 32, pages 83–98, Montreal, CANADA, 2009. Elsevier. 34

J E Shepherd. Ignition Modeling and the Critical Decay Rate Concept. GALCIT Report EDL2019.002, California Institute of Technology, Pasadena, California, February 2020. 3, 6, 22

R.I. Soloukhin. Nonstationary phenomena in gaseous detonation. *Sympoisum (International) on Combustion*, 12(1):799–807, 1969. 3

Yaqin Tan, Rémy Mével, and Yu Cheng Liu. A review on ignition in expanding gaseous media. *Process Safety and Environmental Protection*, 179:241–256, November 2023. 3

C Vázquez-espí and A Liñán. Fast, non-diffusive ignition of a gaseous reacting mixture subject to a point energy source. *Combustion Theory and Modelling*, 5(3):485–498, September 2001. 3

P. Vidal and B.A. Khasainov. Analysis of critical dynamics for shock-induced adiabatic explosions by means of the Cauchy problem for the shock transformation. *Shock Waves*, 9(4):273–290, August 1999. 3

A ZND Reaction Zone Structure

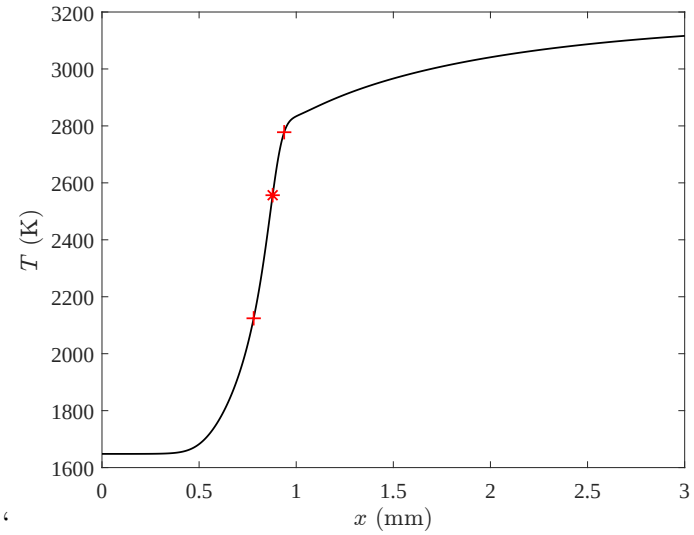

Figure 21: Temperature profile for ZND reaction model of CJ detonation in CH_4-$2O_2$-$2.5N_2$ mixture at 18.8 kPa and 295 K initial conditions. The star symbol indicates the thermicity peak location and the crosses indicate the thermicity 50% locations. The temperature rise after 1 mm is due to the slow recombination of the non-equilibrium concentrations of radicals and intermediate species following the consumption of fuel in the energy release zone.

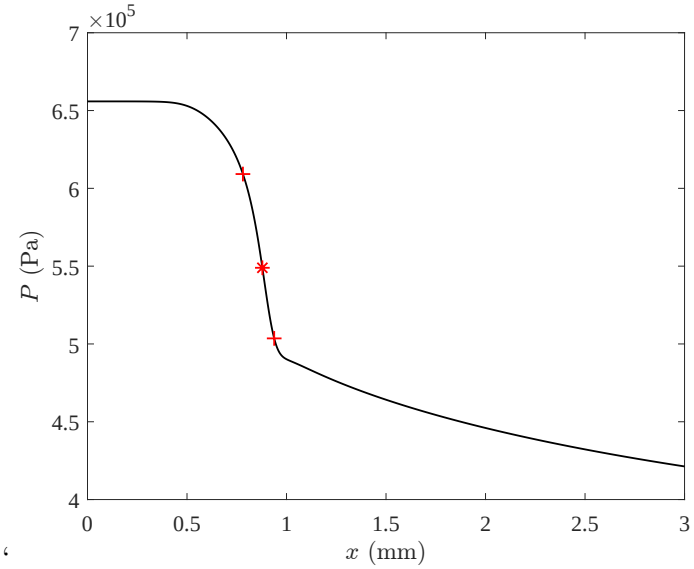

Figure 22: Pressure profile for ZND reaction model of CJ detonation in CH_4-$2O_2$-$2.5N_2$ mixture at 18.8 kPa and 295 K initial conditions.

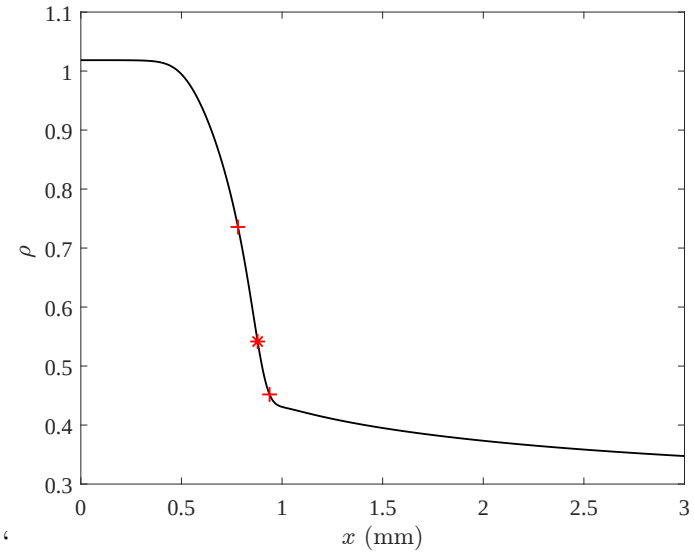

Figure 23: Density profile for ZND reaction model of CJ detonation in CH_4-$2O_2$-$2.5N_2$ mixture at 18.8 kPa and 295 K initial conditions.

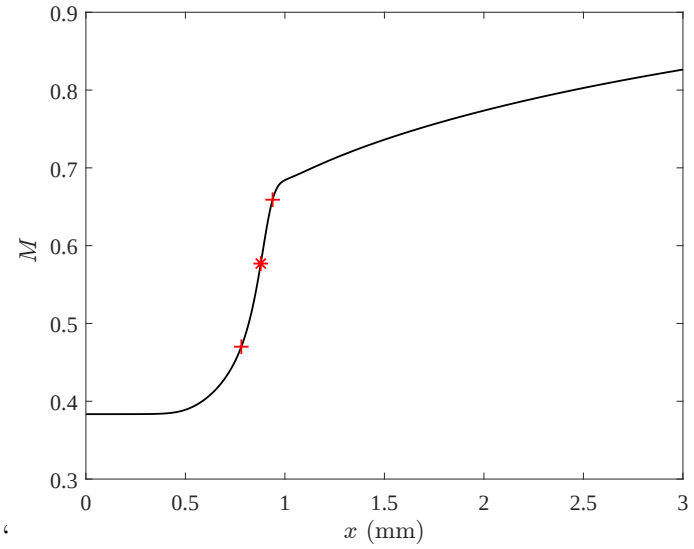

Figure 24: Mach number profile for ZND reaction model of CJ detonation in CH_4-$2O_2$-$2.5N_2$ mixture at 18.8 kPa and 295 K initial conditions.

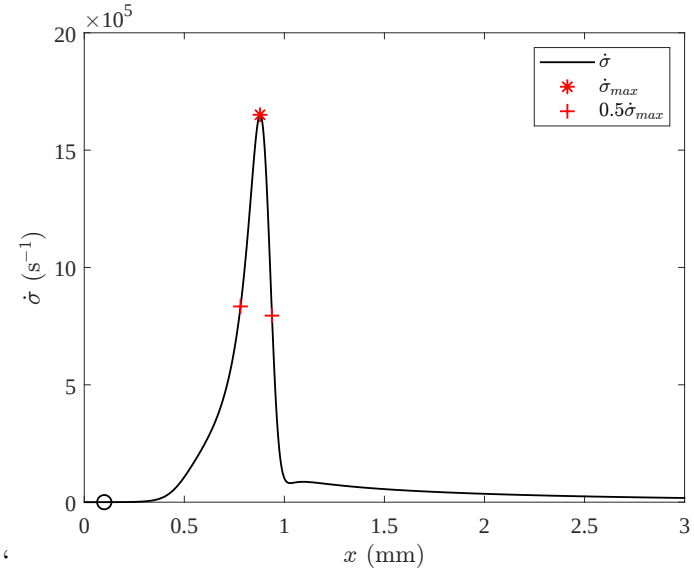

Figure 25: Thermicity profile for ZND reaction model of CJ detonation in CH_4-$2O_2$-$2.5N_2$ mixture at 18.8 kPa and 295 K initial conditions.

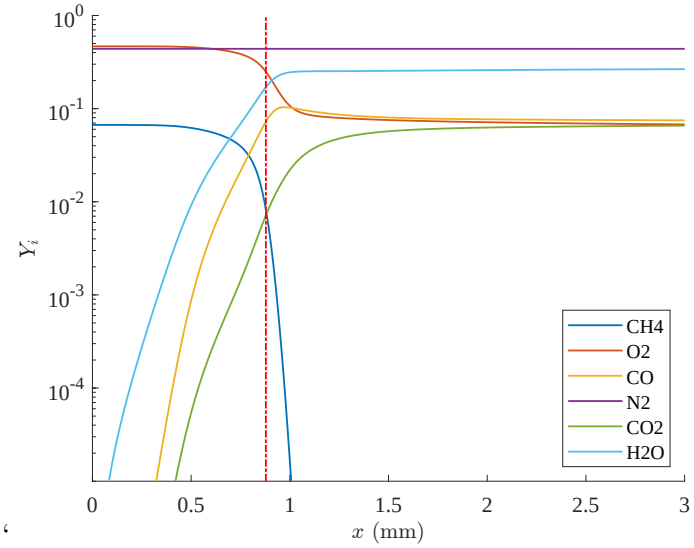

Figure 26: Major species profile for ZND reaction model of CJ detonation in CH_4-$2O_2$-$2.5N_2$ mixture at 18.8 kPa and 295 K initial conditions. The vertical line indicates the location of the the thermicity peak.

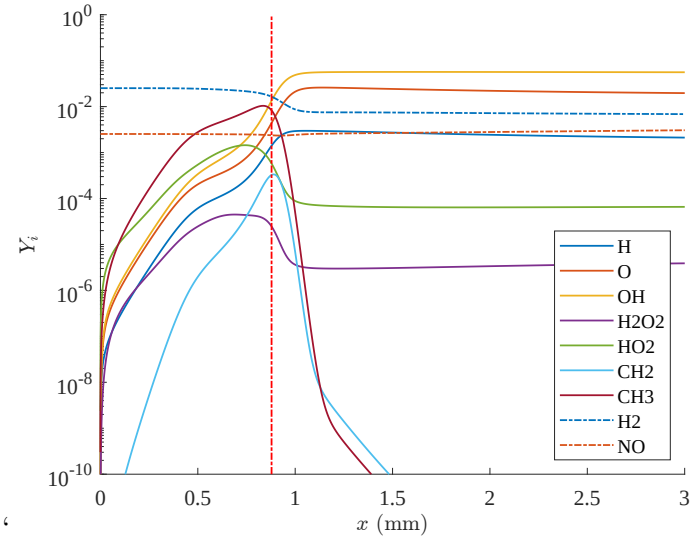

Figure 27: Major species profile for ZND reaction model of CJ detonation in CH_4-$2O_2$-$2.5N_2$ mixture at 18.8 kPa and 295 K initial conditions.